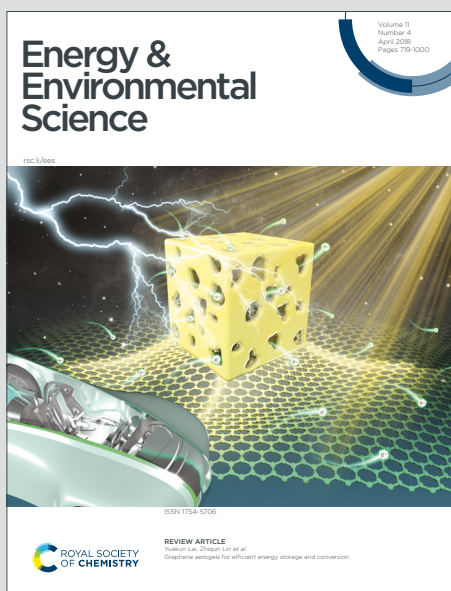


# Energy & Environmental Science

Accepted Manuscript

This article can be cited before page numbers have been issued, to do this please use: R. Roy, M. M. Byranvand, M. Zohdi, T. Magorian Friedlmeier, C. Das, W. Hempel, W. Zuo, M. Kedia, J. J. Jerónimo-Rendon, S. Boehringer, B. Hailegnaw, M. Vorochta, S. Mehl, M. Rai, A. Kulkarni, S. Mathur and M. Saliba, *Energy Environ. Sci.*, 2025, DOI: 10.1039/D4EE02385D.



This is an Accepted Manuscript, which has been through the Royal Society of Chemistry peer review process and has been accepted for publication.

Accepted Manuscripts are published online shortly after acceptance, before technical editing, formatting and proof reading. Using this free service, authors can make their results available to the community, in citable form, before we publish the edited article. We will replace this Accepted Manuscript with the edited and formatted Advance Article as soon as it is available.

You can find more information about Accepted Manuscripts in the [Information for Authors](#).

Please note that technical editing may introduce minor changes to the text and/or graphics, which may alter content. The journal's standard [Terms & Conditions](#) and the [Ethical guidelines](#) still apply. In no event shall the Royal Society of Chemistry be held responsible for any errors or omissions in this Accepted Manuscript or any consequences arising from the use of any information it contains.

# Broader Context Statement:

Metal halide perovskites have achieved a significant milestone by reaching  $> 26\%$  efficiency in recent years. Along with that, the remarkable stability improvement of the perovskite solar cell (PSC) in the recent years makes it more industry friendly.

All-inorganic PSCs (AIPSC) have emerged as one of the promising candidates due to the robustness of its precursors. However, the stability remains one of the major concerns for the AIPSCs. In this article, we have incorporated a polymeric protection layer over the perovskite layer to overcome this issue. We have performed various stability tests under high temperature and high humidity along with direct exposure of the perovskite films to water. In addition, the devices have also shown impressive performance.



# All-inorganic CsPbI<sub>2</sub>Br Perovskite Solar Cells with Thermal Stability at 250 °C and Moisture-Resilience via Polymeric Protection Layers

View Article Online  
DOI: 10.1039/D4EE02385D

Rajarshi Roy,<sup>1</sup> Mahdi Malekshahi Byranvand,<sup>1\*</sup> Mohamed Reza Zohdi<sup>1</sup>, Magorian Friedlmeier Theresa<sup>3</sup>, Chittaranjan Das<sup>1</sup>, Wolfram Hempel<sup>3</sup>, Weiwei Zuo<sup>1</sup>, Mayank Kedia<sup>1,2</sup>, Jose Jeronimo Rendon<sup>1</sup>, Stephan Boehringer<sup>1</sup>, Bekele Hailegnanw<sup>1</sup>, Michael Vorochta<sup>5</sup>, Sascha Mehl<sup>6</sup>, Monika Rai<sup>1,7</sup>, Ashish Kulkarni<sup>2,4\*</sup>, Sanjay Mathur<sup>4</sup>, Michael Saliba<sup>1,2\*</sup>

<sup>1</sup>Institute for Photovoltaics (*ipv*), University of Stuttgart, 70569 Stuttgart, Germany

<sup>2</sup>Helmholtz Young Investigator Group FRONTRUNNER, IEK-5 Photovoltaics, Forschungszentrum Jülich, 52425 Jülich, Germany

<sup>3</sup>Photovoltaics: Materials Research, Zentrum für Sonnenenergie- und Wasserstoff-Forschung (ZSW), 70563, Stuttgart, Germany

<sup>4</sup>Institute of Inorganic Chemistry, University of Cologne, Greinstr. 6, 50939 Cologne, Germany

<sup>5</sup> Faculty of Mathematics and Physics, Charles University, V Holešovičkách 2, Prague 8, 18000 Prague, Czech Republic

<sup>6</sup>Elettra Sincrotrone, Strada Statale 14 km, 34149 Basovizza, Trieste, Italy

current address: <sup>7</sup>Institute for Materials Research (IMO-IMOMEC), University of Hasselt, 3590 Diepenbeek, Belgium

Email: [mahdi.malekshahi@ipv.uni-stuttgart.de](mailto:mahdi.malekshahi@ipv.uni-stuttgart.de), [a.kulkarni@fz-juelich.de](mailto:a.kulkarni@fz-juelich.de),  
[michael.saliba@ipv.uni-stuttgart.de](mailto:michael.saliba@ipv.uni-stuttgart.de)

## Abstract

All-inorganic perovskites, such as CsPbI<sub>2</sub>Br, have emerged as promising compositions due to their enhanced thermal stability. However, they face significant challenges due to their susceptibility to humidity. In this work, CsPbI<sub>2</sub>Br perovskite is treated with poly(3-



hexylthiophen-2,5-diyl) (P3HT) during the crystallization resulting in significant stability improvements against thermal, moisture and steady-state operation stressors. The perovskite solar cell retains ~90% of the initial efficiency under relative humidity (RH) at ~60% for 30 min, which is among the most stable all-inorganic perovskite devices to date under such harsh conditions. Furthermore, the P3HT treatment ensures high thermal stress tolerance at 250 °C for over 5 h.

In addition to the stability enhancements, the champion P3HT-treated device shows a higher power conversion efficiency (PCE) of 13.5% compared to 12.7% (reference) with the stabilized power output (SPO) for 300 s. In addition, the P3HT-protected perovskite layer in ambient conditions shows ~75% of the initial PCEs compared to the unprotected PSCs with ~28% of their initial PCEs for 7 days of shelf-life.

**KEYWORDS:** Inorganic perovskite, P3HT, interlayer, solar cell, high stability.

## INTRODUCTION

Perovskite solar cells (PSCs) have garnered significant interest due to their excellent optoelectronic properties and high power conversion efficiencies (PCEs), which have increased from 3.8%<sup>[1]</sup> in 2009 to >26%<sup>[2]</sup> to date. The potential commercial viability of this technology is being evaluated due to recent advances in perovskite material structural and environmental stability achieved through compositional, interfacial, and additive engineering.<sup>[3-15]</sup> While improvements have been made in the moisture stability of organic-inorganic perovskites, concerns about low thermal stability persist, particularly due to the presence of volatile organic cations.<sup>[16]</sup> This concern has led to increased research focused on all-inorganic perovskites incorporating the cesium (Cs) cation (CsPbX<sub>3</sub>; X = I, Br). Recent studies have achieved impressive PCEs for CsPbI<sub>3</sub><sup>[17,18]</sup> and CsPbI<sub>2</sub>Br<sup>[19,20]</sup> PSCs of 19.6% and 17.8%, respectively. However, there are still stability concerns that persist. To increase confidence in the principled long-term thermal stability of PSCs, stability against extreme temperatures > 400 °C, as achievable by all-inorganic perovskites, would be an important milestone, also for space



applications. In this work, carrying out the similar thermal stability traits, we have performed robust moisture stability tests to verify our interface engineering strategy.

The more crucial concern, rather than thermal degradation or chemical decomposition in a humid environment, lies in the inherent instability of the photoactive phase of all-inorganic perovskites at room temperature. Among the  $\text{CsPbX}_3$  perovskite compositions,  $\text{CsPbI}_3$  (bandgap of 1.7 eV) exhibits a phase instability at room temperature, i.e. a transition from the photoactive black phase ( $\alpha$ ) to the photoinactive yellow phase ( $\delta$ )<sup>[21]</sup>.  $\text{CsPbBr}_3$ , on the other hand, associated with poor light absorption beyond 540 nm due to its wide bandgap of 2.3 eV.<sup>[22-23]</sup> As a trade-off, a mixed-halide  $\text{CsPbI}_2\text{Br}$  composition shows a lower bandgap of 1.9 eV (with Shockley-Queisser limit of 24.7%) and better phase stability than  $\text{CsPbI}_3$ , thus positioning it as a promising candidate for thermally stable single-junction perovskite solar cells or multijunction applications.<sup>[24]</sup> While studies have shown improvements in phase stability<sup>[25-33]</sup>, achieving stability against moisture (full exposure to water), and heat (>200 °C) remains challenging, necessitating the development of innovative strategies to address these challenges.

In this study, we present an effective strategy to enhance the moisture and thermal stability of the  $\text{CsPbI}_2\text{Br}$  perovskite films through polymer additive-assisted antisolvent engineering. The optimized amount of poly(3-hexylthiophen-2,5-diyl) (P3HT) polymer is introduced during the antisolvent dripping step, improving the perovskite crystallization in the presence of P3HT. Our characterizations confirm the formation of a thin P3HT layer and the formation of  $\text{CH}_3\text{Br}$  organic adduct on the surface of the perovskite film, respectively. This may also contribute to the enhancement of the interfacial junction between the perovskite and the HTL, leading to the device stability improvement. This may stem from the reduction of dangling bonds on the surface of perovskite film, thus achieving a better interface. Upon exposure to moisture at room humidity (RH) ~ 60% for 30 min, the devices retained 90% of their initial PCE. Additionally, when subjected to heating at 250 °C under ambient conditions for 300 min the devices retained ~ 50% of their initial PCE. As high temperature creates an area free of moisture as well as due to the high temperature tolerance of the perovskite layer, we have performed the high temperature assisted robust stability tests in this work. In addition to this, the shelf-life stability data demonstrates that, on average, the devices retained ~ 75% of their initial PCE for 7 consecutive days of measurement under 1-sun condition. The P3HT-treated device exhibited a notable enhancement in the fill factor (FF), > 82%, compared to the reference device (without

View Article Online  
DOI: 10.1039/D4EE02385D



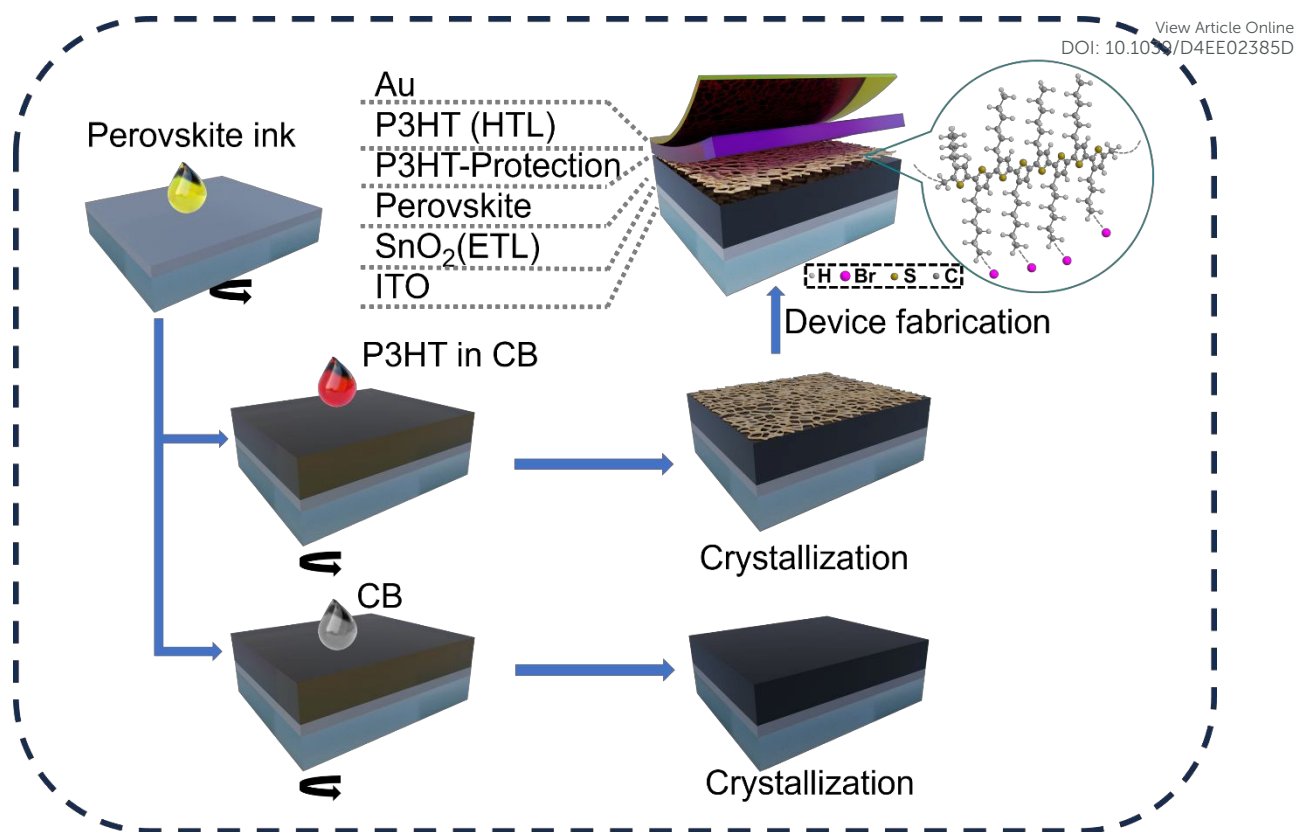
any treatment) with a FF of 79% underlining the improved interface resulting from the P3HT treatment. Article Online  
DOI: 10.1039/D4EE02385D

## Results and discussions

As shown in Schematic 1 our results are based on an *n-i-p* stack of indium tin oxide (ITO) glass/nanoparticle-based SnO<sub>2</sub> electron transport layer (ETL)/ CsPbI<sub>2</sub>Br film (with and without P3HT-protection)/ P3HT HTL/gold metal electrode. For the P3HT-protected devices, varying concentrations of P3HT in CB are dissolved and dripped (as an antisolvent) during the perovskite precursor spin coating step, followed by annealing on a hot plate to facilitate perovskite crystallization. This modification process leads to the formation of a P3HT protection layer at the interface of perovskite and HTL.

For P3HT-protection layer modification, from various film characterizations such as the XRD (**Figure S1**), SEM top-view (**Figure S2**) and from the device statistics (**Figure S3**) that 6mg/mL of P3HT-protection layer concentration to be the optimum and carried on further characterizations. From here, for convenience, the perovskite devices and films modified with this P3HT interlayer concentration as the ‘P3HT-protected’ in comparison to the unmodified one as ‘unprotected’.





**Schematic 1.** Schematic illustration of perovskite film processing and PSC device with and without P3HT-protection layer

To analyse the influence of P3HT interlayer on the perovskite layer absorbance we carried out UV-vis absorption measurements. The absorption spectra in **Figure 1A** show no change in absorbance between the unprotected and the P3HT-protected substrates, indicating that the P3HT interlayer at varying concentrations does not affect the optical properties of perovskite film (**Figure S4**). Additionally, the XRD measurement (**Figure 1B**) reveals major characteristic peaks at  $2\theta = 14.6^\circ$  and  $29.8^\circ$ , corresponding to the  $\alpha$  phase of the perovskite, with no traces of  $\delta$  phase at  $\sim 10^\circ$ . Interestingly, the perovskite peak intensity is slightly higher with lower Full Width at Half Maximum (FWHM) (**Figure S5**) for the P3HT-protected compared to the unprotected. We posit that this is primarily due to the formation of a better interface between the perovskite absorber layer and the HTL by the P3HT treatment. This additionally results in obtaining the perovskite layer with fewer defects, leading to better crystalline film. From the SEM images in **Figure 1C**, the unprotected film exhibits a non-flat surface with high coverage, which transforms into a fully covered morphology with the addition of the P3HT layer on top of it (**Figure 1D**). The effect of the P3HT protection over





the perovskite layer is further evident from the atomic force microscopy (AFM) images for the unprotected and P3HT-protected films in **Figures 1G, 1H**. The root mean square (RMS) roughness of the perovskite film has decreased from  $18 \pm 1$  nm for the unprotected to  $12 \pm 1$  nm when crystallized in the presence of P3HT, resulting in a more uniform perovskite layer. The uniformity is further verified by the surface SEM as shown in **Figure S6**. In comparison to unprotected perovskite film (with an average grain size of 104 nm), the P3HT-protected perovskite film has shown a smaller grain size of 95 nm which also implements the improved interface of the latter. Photoluminescence (PL) measurements were carried out to quantify the charge transport properties at the perovskite and P3HT interlayer interface. As depicted in **Figure 1E**, the P3HT-protected film shows significant PL quenching compared to the unprotected film, suggesting fast charge extraction attributable to the P3HT interlayer compared to the unprotected film. This is further suggested by the Time-resolved photoluminescence (TRPL) measurement. TRPL measurement is performed to further understand the carrier transfer dynamics at the perovskite/HTL interface, and the results are shown in **Figure 1F**. The TRPL curves are fitted with the biexponential decay function as shown in **Table S1**.

$$I(t) = A_1 \exp\left(-\frac{t}{\tau_1}\right) + A_2 \exp\left(-\frac{t}{\tau_2}\right) + K$$

Here,  $A_1$  and  $A_2$  are the decay amplitude,  $\tau_1$  and  $\tau_2$  are the characteristic time constants for the first and second exponential decays respectively.  $K$  is a constant for the base-line offset. Here we emphasize that the characteristic time constants which are obtained from the biexponential fitting, solely represent the fitting parameters which are further used to understand the PL decay for the unprotected and P3HT-protected films. Here during the analysis,  $\tau_1$  and  $\tau_2$  have represented the characteristic decay times which are driven by factors such as, trap states or charge extraction, but they do not necessarily represent the charge-carrier lifetimes for the unprotected and P3HT-protected films. Since there is no charge extraction in the unprotected film,  $\tau_1$  represents the recombination in trap states. Where as in the P3HT-protected film the decay time is dominated more by the charge extraction rather than the trap states. As charge extraction does not lead to radiative recombination, therefore the PL yield is reduced for the P3HT-protected film compared to the unprotected film as observed by the steady-state PL measurement. Although the decay curve  $\tau_1$  for the P3HT-protected film does not prove that the charge carriers are extracted, it is the most probable mechanism since otherwise the fast decay would mean the loss of carriers in trap states. As a result, this would lead to a non-functioning





device, which is not the case in our study. Faster charge extraction as well as reduced trap-induced non-radiative recombination in the interface suggests that a better interface can be obtained by incorporating a P3HT interlayer between the perovskite and the HTL, thereby improving charge transport properties and device performance. We employed both laboratory and synchrotron XPS methods for surface-to-bulk chemical analysis (**Figures 1I, 1J**) to realize the effect of the protection layer over the perovskite surface. Unlike the unprotected perovskite films, a distinct peak at  $\sim 71.9$  eV is observed along with the Br3d (69.0 eV) and Cs3d (76.2 eV) in the XPS spectra of P3HT-protected perovskite films, with higher intensity at lower photon energy, indicating surface phenomena. This peak likely originates from an organic adduct, such as  $-\text{CH}_3\text{Br}$ , formed from the reaction between P3HT's  $-\text{C}_6\text{H}_{13}$  side chain and excess Br during perovskite layer formation<sup>[34]</sup>. The surface-bound adduct potentially reduces dangling bonds from undercoordinated lead atoms, thereby decreasing surface recombination and enhancing interfacial charge transport and stability. For the work function (WF) analysis and corresponding binding energies (C1s, Pb4f, S2p, I3d) please refer to **Figure S7**. We have also analysed the depth profile between the perovskite and the P3HT layer via the Time of Flight Secondary Ion Mass Spectrometry (ToF-SIMS) measurements (**Figure S8**). The ToF-SIMS measurement shows that the overall layer depth of the perovskite composition remains the same. The increase in the amount of lead at the surface may stem from the matrix effect. Notably, the presence of Sulphur in the form of  $-\text{SCH}^+$  species and the hydrocarbon chain ( $\text{C}_6\text{H}_6$ ) was exclusively observed at the P3HT-protected sample surface. Additionally, a signal from a  $[\text{PbOSCH}]^+$  cluster on the surface of the P3HT-protected perovskite layer is observed as reported in **Figure S8**. Thus, the interaction between  $\text{Pb}^{2+}$  and  $\text{SCH}^+$  on the surface appears to reduce the non-radiative recombination as well as improved stability.

View Article Online  
DOI: 10.1039/C4EE02385D



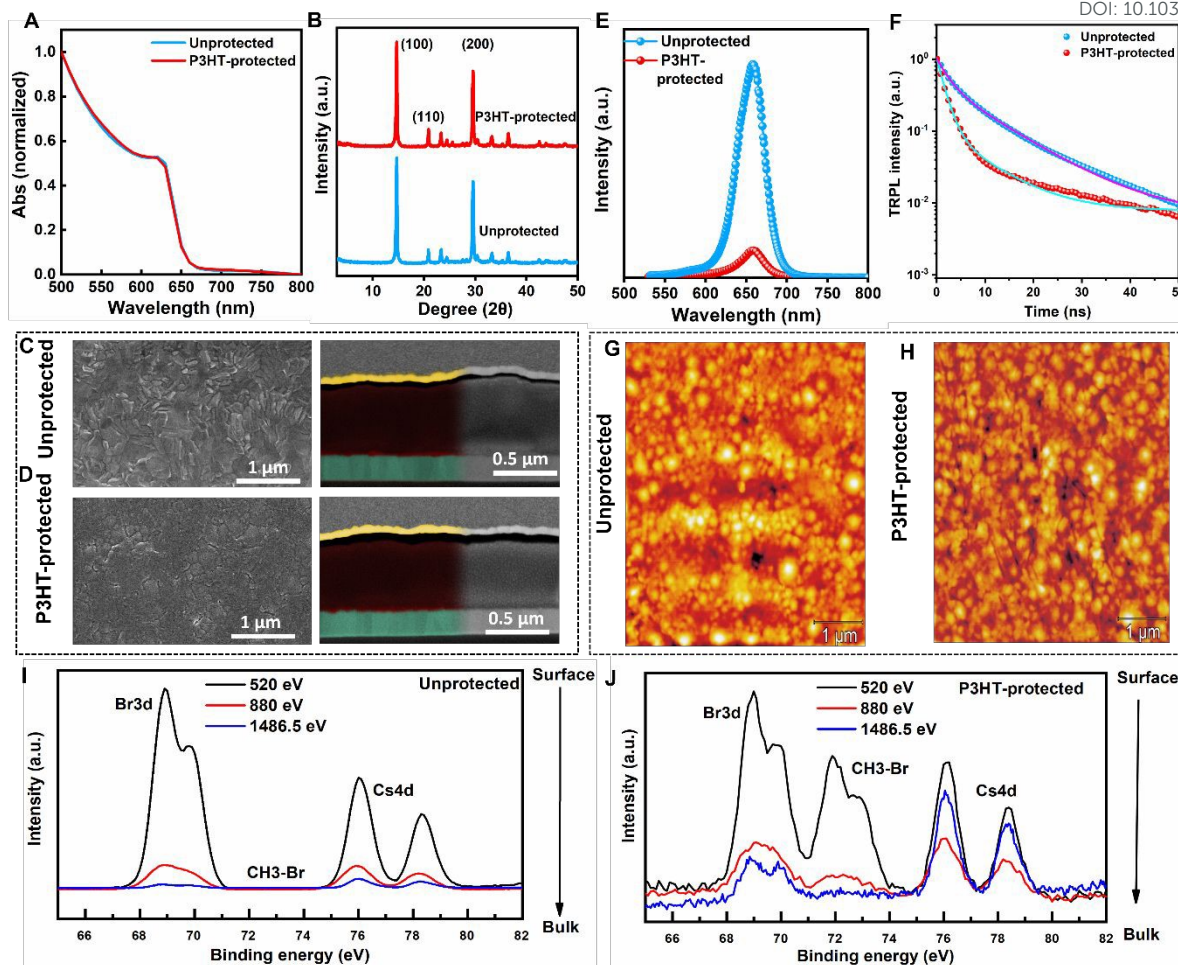


**Figure 1.** (A) UV-Vis absorption spectra of unprotected film and P3HT-protected film. (B) XRD spectra (C), (D) Surface and cross-sectional SEM images, (E) steady-state PL spectra, (F) TRPL spectra, (G) and (H) AFM images of the unprotected and P3HT-protected films, (I) and (J) XPS measurement of Cs (4d) Br (3d) at 520 eV, 880 eV and 1486.5 eV for the unprotected film and P3HT-protected film

In addition to the phase stability, one of the main hurdles for the all-inorganic perovskite is stability against high temperature and humidity. Therefore, we have investigated the stability improvement of the perovskite films under different conditions, such as high humidity (~60%), high thermal stress of 250 °C, and by dipping the perovskite films in water. For the humidity test, the structural stabilities of the unprotected and P3HT-protected perovskite films were evaluated using the X-ray diffraction (XRD) measurements, and the results are shown in **Figure 2A** and **Figure 2B**, respectively. For fresh samples, the XRD measurements are performed directly after the deposition for both the unprotected and P3HT-protected films. To



test the stability of perovskite films (unprotected and P3HT-protected) against humidity, the XRD measurement was carried out after aging for 30 min (with 10 min time intervals) in a closed controlled chamber with RH ~ 60%. As can be seen in **Figure 2A**, for the unprotected films, after aging for 10 min in RH ~60%, the XRD pattern shows the appearance of the  $\delta$  phase peak at  $2\theta = 10.6^\circ$  indicating the degradation of the perovskite black phase. The XRD peak intensity of  $\delta$  phase increases with further aging. After 30 min of aging, the  $\alpha$  phase of the perovskite deteriorates completely as the peak at  $2\theta = 14.6^\circ$  significantly reduces and a strong intense peak corresponding to the degraded yellow phase appears. On the other hand, for the P3HT-protected perovskite film, the XRD pattern shows negligible change in the XRD peak intensity at  $2\theta = 14.6^\circ$  and  $29.8^\circ$ , implying enhanced stability. Furthermore, it's worth noting that only a minimal amount of the  $\delta$  phase forms after a 30 min aging period, as shown in **Figure 2B**. Along with the  $\delta$ -phase peak, the formation of the  $\text{PbI}_2$  peak also emerges at  $2\theta = 12.6^\circ$  for the unprotected devices with aging. However, in the case of the P3HT-protected films, the formation of the  $\text{PbI}_2$  peak is negligible even after 30 min of aging. The slower formation of the  $\delta$ -phase peak and  $\text{PbI}_2$  peak at RH ~ 60% emphasizes the improved perovskite stability and film quality attributed to the presence of the P3HT interlayer. This improvement is further supported by the contact angle measurement under ambient conditions as shown in **Figure S9**.

For the thermal stability tests, the XRD is recorded by exposing the unprotected and P3HT-protected films to  $250^\circ\text{C}$  under ambient humidity conditions. The results are shown in **Figure 2C** and **Figure 2D**, respectively. Under high thermal stress, the unprotected perovskite films transform from the photoactive black phase to the photoinactive yellow phase while the P3HT-protected perovskite film shows a stable black phase even after 300 min of exposing to high temperature.



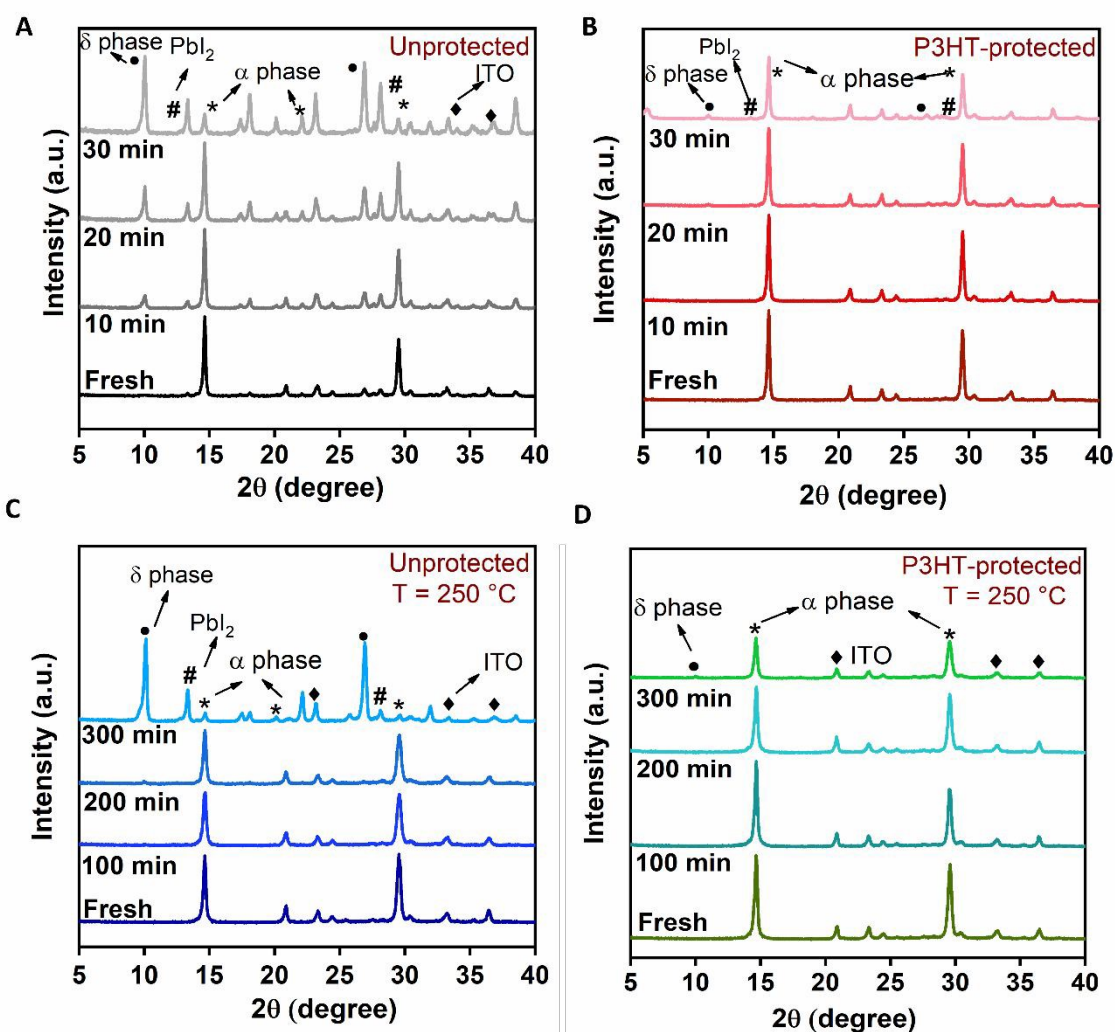


**Figure 2.** XRD pattern of (A) unprotected and (B) P3HT-protected perovskite films under 60% humidity conditions, (C) and (D) unprotected and P3HT-protected perovskite films under thermal stress

To access the stability enhancement through the P3HT interface engineering, we have conducted the water dipping test on the films. **Figures. 3A, 3C** show the effect of P3HT-protection layer when dipped in water compared to the unprotected. **Figures. 3B, 3D** show the XRD pattern for the unprotected and P3HT-protected films respectively after dipping in water. The P3HT-protected film has retained the perovskite layer for more than 30 s without significant change in the colour compared to the unprotected which has shown a rapid colour change from brown to yellow after 5 s submersion in water. This observation is supported by the corresponding XRD plots. Upon water dipping, the unprotected film (**Figure. 3B**) exhibited





a  $\delta$  peak at  $10.6^\circ$  and a  $\text{PbI}_2$  peak at  $12.6^\circ$  immediately, with a degraded perovskite peak. After 10 s, the unprotected film shows complete degradation with a highly intense  $\text{PbI}_2$  peak. In contrast, the P3HT-protected film, after 5 s of dipping, displays only a negligible amount of degradation with a small amount of  $\text{PbI}_2$  peak while maintaining a strong intense perovskite peak at  $14.6^\circ$ , indicating the additional stability provided by the P3HT interlayer (**Figure. 3D**). Continued water exposure led to a gradual degradation of the perovskite peak after 30 s for the P3HT-protected film, accompanied by the appearance of the  $\text{PbI}_2$  peak at  $12.6^\circ$  and the  $\delta$  peak. This indicates that the incorporation of the P3HT interlayer during the perovskite crystallization plays a significant role in providing additional stability to the perovskite layer by shielding it from exposure to water molecules.

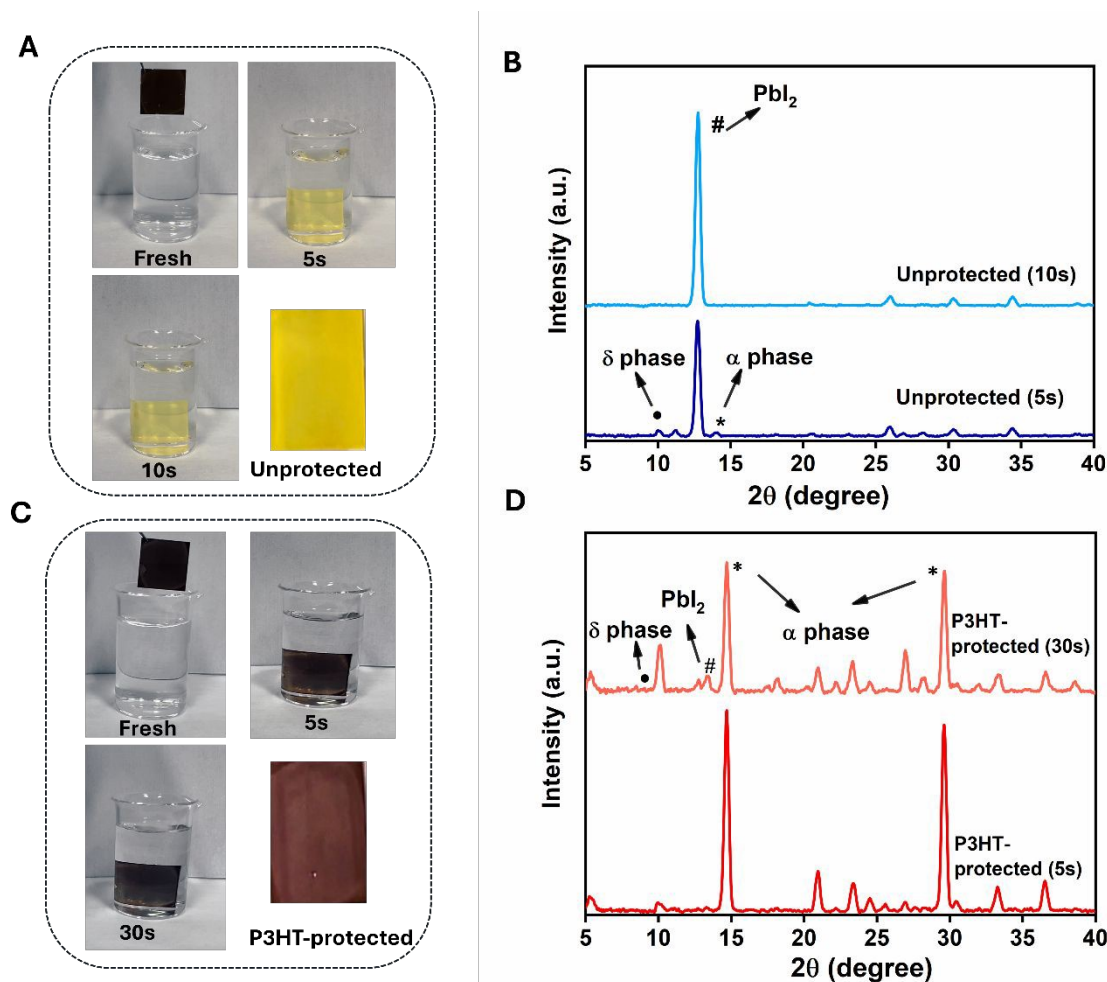


**Figure 3.** (A) Water dipping test for the unprotected film. (B) XRD pattern of the unprotected film post dipping. (C) Water dipping test for the P3HT-protected film (D) XRD pattern of the P3HT-protected film post dipping



The device processing is outlined and explained in Schematic 1. **Figures 4A, 4B, 4C, 4D** represent the device statistics and shows a significant increase in all the device parameters especially in the FF. The unprotected PSCs show an average short-circuit current ( $J_{SC}$ ) = (12.5 ± 0.5) mA/cm<sup>2</sup> (n=38), open-circuit voltage ( $V_{OC}$ ) = (1.13 ± 0.03) V, and  $FF$  = (73.0 ± 5.0) % and PCE of (11 ± 1.7) % where the P3HT-protected devices show an average  $J_{SC}$  = (13.5 ± 0.8) mA/cm<sup>2</sup> (n=44),  $V_{OC}$  = (1.15 ± 0.6) V,  $FF$  = (79 ± 2.0) % and PCE of (11 ± 2.3) %. **Figure 4E** shows the best-performing current density-voltage ( $J$ - $V$ ) characteristic curves of the unprotected and P3HT-protected devices (measured under the reverse scan) along with the stabilized power output (SPO) measurement over 300 seconds under 1-sun illumination. The best-performing device parameters for unprotected and P3HT-protected devices are presented in **Table 1**.

**Table 1. Measured PV parameters for the best-performing unprotected and P3HT-protected device**

Device	$J_{SC}$ (mA/cm <sup>2</sup> )	$V_{OC}$ (V)	FF (%)	PCE (%)
<b>Unprotected</b>	13.6	1.17	79.6	12.7
<b>Average photovoltaic parameters</b>	12.5 ± 0.5	1.13 ± 0.03	73.0 ± 5.0	11 ± 1.7
<b>Median</b>	12.55	1.15	73.31	11.00
<b>P3HT-protected</b>	14.0	1.17	82.2	13.5
<b>Average photovoltaic parameters</b>	13.5 ± 0.8	1.15 ± 0.6	79 ± 2.0	11 ± 2.3
<b>Median</b>	13.31	1.16	78.30	12.23

The significant FF improvement is likely due to the enhanced interfacial connection between the perovskite and the HTL via the P3HT protection layer, as well as reduced surface recombination. In addition to the FF, there is also a slight increase in the photocurrent for the devices with the P3HT-protection layer (14 mA/cm<sup>2</sup>), aligning well with the  $J_{SC}$  (13.6 mA/cm<sup>2</sup>) obtained from the external quantum efficiency (EQE) measurement, as shown in **Figure S10**, implying excellent hole transport capability via the P3HT protection and emphasizing the role of charge transport layer in enhancing the  $J_{SC}$ <sup>[35]</sup>. Additionally, to explore the impact of the P3HT-protection layer in the presence of another HTL, devices were fabricated using Spiro-MeOTAD as the HTL, as illustrated in **Figure S11**, and **Figure S12**. In addition, the device



stability test has been performed under 80 ° C for the P3HT-protected devices and unprotected devices (with P3HT or, spiro as HTL) as shown in **Figure S13**. The stability test is performed in ambient condition for 450 mins retaining > 90% of the  $PCE_{Initial}$  and in  $N_2$  condition for 100 h retaining ~ 80% of the  $PCE_{Initial}$  for the P3HT-protected devices. However, the overall device performance is notably superior when using P3HT as the HTL with the P3HT-protection layer. **Figure 4F** represents the shelf-life stability of the unprotected and P3HT-protected devices over 7 days of measurement in ambient humidity conditions. P3HT-protected devices have retained ~75% of their initial PCE, while the unprotected devices retain only ~28% of their initial value. To further understand the effect of stability on the device performance, we have fabricated  $CsPbI_2Br$  devices based on unprotected and P3HT-protected films under RH~60%. P3HT-protected perovskite films retained ~ 90% of the initial PCE while the unprotected devices completely degraded after the aging test as shown in **Figure 4G**. This corroborates the XRD pattern (**Figures. 2A, 2B**) and signifies the importance of the P3HT-protection layer to enhance the stability of the inorganic perovskite against high humidity atmosphere. To understand the prolonged stability of P3HT-protected perovskite thin films, we fabricated devices with perovskites exposed to 250 °C and performed the thermal  $J-V$  measurements in **Figure 4H**. As can be seen, the aged P3HT-protected device still retained more than 50% of its initial PCE after aging for 300 min whereas for the unprotected devices, the average PCE decreased to less than 25% after the thermal aging test. These results correspond well with the thermal XRD data as shown earlier in **Figures. 2C, 2D** followed by gives us a strong implication on the stability improvement with the P3HT-protection layer under robust conditions and stress factors. The role of P3HT-protection layer is further tested over devices with spiro HTL at RH ~ 60% and temperature at 80 ° C as shown in **S14**. The devices with P3HT-protection layer showed better stability compared to the unprotected, implying the efficacy of the interface engineering strategy over other HTM.

View Article Online  
DOI:10.1039/D4EE02385D





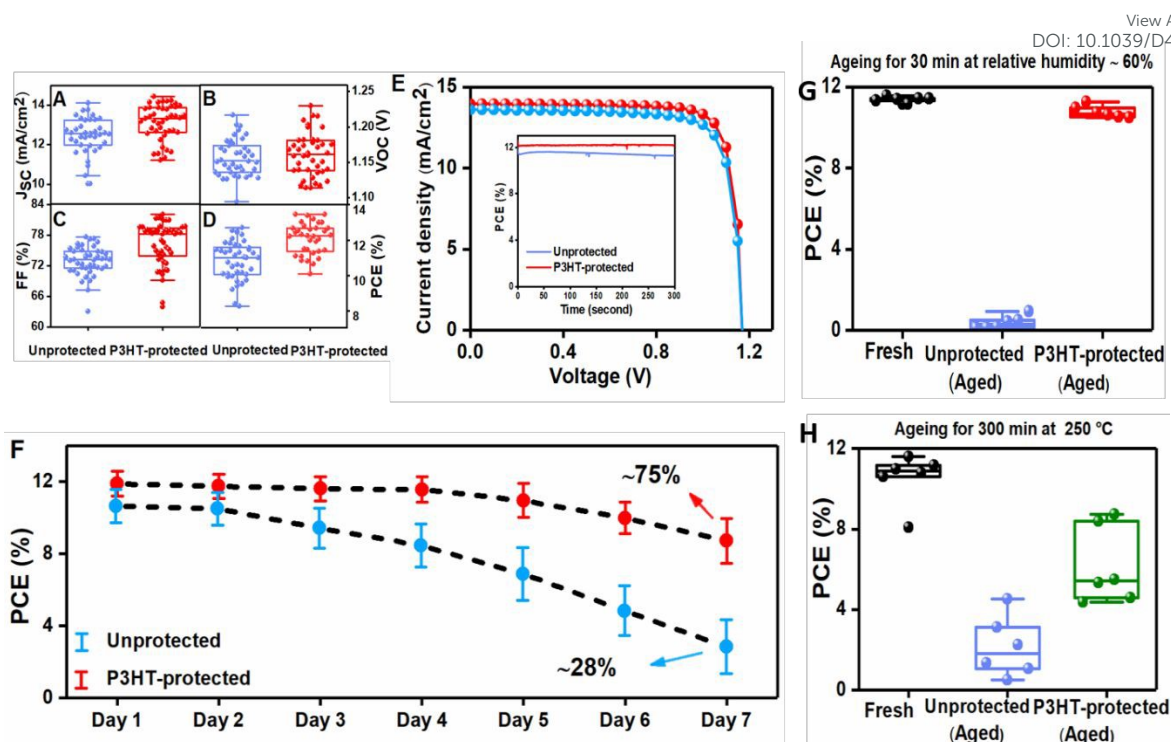


**Figure 4:** (A, B, C, D) Device statistics ( $n = 38$ ) of the unprotected and P3HT-protected devices ( $n = 44$ ) for current density, open-circuit voltage, fill factor, and power conversion efficiency, (E)  $J-V$  curves for the best performing unprotected and P3HT-protected device along with the stabilized power output (SPO) of the respective devices, (F) Shelf-life stability of the unprotected and P3HT-protected devices over 7 days of  $J-V$  measurement, (G) Device statistics for the unprotected and P3HT-protected at RH~60%, (H) Device statistics for the unprotected and P3HT-protected under thermal stress of 250 °C

### Conclusion:

Our study develops an interface strategy for enhancing the stability of the all-inorganic perovskite composition (CsPbI<sub>2</sub>Br). The deposition of a thin layer of P3HT between the perovskite and the hole transport layer proved to be instrumental in improving the film morphology and crystallinity as evident from the SEM and XRD analyses, respectively. ToF-SIMS studies reveal the presence of P3HT layer only on top of the perovskite layer with no traces in the bulk. XPS analysis, along with the PL and TRPL results, signifies a significant reduction in surface recombination and overall enhancement in the interfacial charge transport



properties and FF up to 82.2%. Humidity XRD tests (RH ~ 60%) demonstrate a significant slowdown in the  $\alpha$  to  $\delta$  phase transition for the P3HT-protected films which is reflected in the device performances, retaining an impressive 90% of their original PCE. Thermal XRD tests at 250 °C, supported by device performance under similar conditions, show the P3HT-protected devices retain more than 50% of their initial PCE value upon 300 min of the aging test. The water dipping test provides clear evidence of the homogeneous surface coverage achieved through P3HT interface strategy, resulting in a more stable perovskite absorber layer. Our findings present an effective route to enhance the stability of the CsPbI<sub>2</sub>Br perovskite solar cells under challenging conditions, such as moisture and high temperature, by slowing down the  $\alpha$  to  $\delta$  phase transition and reduced surface recombination.

## ACKNOWLEDGEMENTS

M.S. and R.R. acknowledge funding by ProperPhotoMile. Project ProperPhotoMile is supported under the umbrella of SOLAR-ERA.NET Cofund 2 by the Spanish Ministry of Science and Education and the AEI under the project PCI2020-112185 and CDTI project number IDI-20210171; the Federal Ministry for Economic Affairs and Energy on the basis of a decision by the German Bundestag project numbers FKZ 03EE1070B and FKZ 03EE1070A and the Israel Ministry of Energy with project number 220-11-031. SOLAR-ERA.NET is supported by the European Commission within the EU Framework Programme for Research and Innovation HORIZON 2020 (Cofund ERA-NET Action, No. 786483), funded by the European Union. The views and opinions expressed are, however, those of the author(s) only and do not necessarily reflect those of the European Union or the European Research Council Executive Agency (ERCEA). Neither the European Union nor the granting authority can be held responsible for them. The authors acknowledge funding from the European Research Council under the Horizon Europe program (LOCAL-HEAT, grant agreement no. 101041809). The authors also thank Somayeh Gholipour for technical assistance. A.K. acknowledge support from Deutscher Akademischer Austauschdienst through a DAAD-PRIME fellowship under the ST43 – Research Fellowship Programmes. M.V acknowledges support from the Czech Ministry of Education, Youth and Sports under the project LM2023072.

## References



1. Kojima, A., Teshima, K., Shirai, Y., & Miyasaka, T. Organometal halide perovskites as visible-light sensitizers for photovoltaic cells. *Journal of the American Chemical Society* **2009**, *131*(17), 6050–6051.
2. National Renewable Energy Laboratory. Best Research-Cell Efficiency Chart | Photovoltaic Research | NREL. <https://www.nrel.gov/pv/cell-efficiency.html>, **2022**.
3. He, F.; Xu, W.; Zhang, M.; Zhang, X.; Ding, B.; Wei, G.; Kang, F. Highly Crystalline CsPbI<sub>2</sub>Br Films for Efficient Perovskite Solar Cells via Compositional Engineering. *RSC Advances* **2019**, *9*, 30534–30540.
4. Chen, Y.; Shi, T.; Liu, P.; Xie, W.; Chen, K.; Xu, X.; Shui, L.; Shang, C.; Chen, Z.; Yip, H.-L.; *et al.* The Distinctive Phase Stability and Defect Physics in CsPbI<sub>2</sub>Br Perovskite. *Journal of Materials Chemistry A* **2019**, *7*, 20201–20207.
5. Bai, D.; Bian, H.; Jin, Z.; Wang, H.; Meng, L.; Wang, Q.; (Frank) Liu, S. Temperature-Assisted Crystallization for Inorganic CsPbI<sub>2</sub>Br Perovskite Solar Cells to Attain High Stabilized Efficiency 14.81%. *Nano Energy* **2018**, *52*, 408–415.
6. Dong, C.; Han, X.; Li, W.; Qiu, Q.; Wang, J. Anti-Solvent Assisted Multi-Step Deposition for Efficient and Stable Carbon-Based CsPbI<sub>2</sub>Br All-Inorganic Perovskite Solar Cell. *Nano Energy* **2019**, *59*, 553–559.
7. Liu, C.; Li, W.; Zhang, C.; Ma, Y.; Fan, J.; Mai, Y. All-Inorganic CsPbI<sub>2</sub>Br Perovskite Solar Cells with High Efficiency Exceeding 13%. *Journal of the American Chemical Society* **2018**, *140*, 3825–3828.
8. Deng, F.; Li, X.; Lv, X.; Zhou, J.; Chen, Y.; Sun, X.; Zheng, Y.-Z.; Tao, X.; Chen, J.-F. Low-Temperature Processing All-Inorganic Carbon-Based Perovskite Solar Cells up to 11.78% Efficiency via Alkali Hydroxides Interfacial Engineering. *ACS Applied Energy Materials* **2019**, *3*, 401–410.
9. Zhang, J.; Jin, Z.; Liang, L.; Wang, H.; Bai, D.; Bian, H.; Wang, K.; Wang, Q.; Yuan, N.; Ding, J.; *et al.* Iodine-optimized Interface for Inorganic CsPbI<sub>2</sub>Br Perovskite Solar Cell to Attain High Stabilized Efficiency Exceeding 14%. *Advanced Science* **2018**, *5*.
10. Lau, C. F.; Zhang, M.; Deng, X.; Zheng, J.; Bing, J.; Ma, Q.; Kim, J.; Hu, L.; Green, M. A.; Huang, S.; *et al.* Strontium-Doped Low-Temperature-Processed CsPbI<sub>2</sub>Br Perovskite Solar Cells. *ACS Energy Letters* **2017**, *2*, 2319–2325.
11. Zhou, L.; Guo, X.; Lin, Z.; Ma, J.; Su, J.; Hu, Z.; Zhang, C.; Liu, S. (Frank); Chang, J.; Hao, Y. Interface Engineering of Low Temperature Processed All-Inorganic CsPbI<sub>2</sub>Br Perovskite Solar Cells toward PCE Exceeding 14%. *Nano Energy* **2019**, *60*, 583–590.



12. Li, J.; Yang, J.; Ma, J.; Liang, J.; Liu, Y.; Hu, X.; Chen, C.; Yang, W.; Min, J.; Bao, Q.; *et al.* Minimizing Open-Circuit Voltage Deficit via Interface Engineering for Highly Efficient CsPbI<sub>2</sub>Br Perovskite Solar Cells. *Chemical Engineering Journal* **2021**, *417*, 129247.
13. Yuan, J.; Zhang, L.; Bi, C.; Wang, M.; Tian, J. Surface Trap States Passivation for High-performance Inorganic Perovskite Solar Cells. *Solar RRL* **2018**, *2*.
14. Jena, A. K.; Kulkarni, A.; Sanehira, Y.; Ikegami, M.; Miyasaka, T. Stabilization of  $\alpha$ -Cspbi3 in Ambient Room Temperature Conditions by Incorporating EU into CsPbI<sub>3</sub>. *Chemistry of Materials* **2018**, *30*, 6668–6674.
15. Öz, S.; Jena, A. K.; Kulkarni, A.; Mouri, K.; Yokoyama, T.; Takei, I.; Ünlü, F.; Mathur, S.; Miyasaka, T. Lead(II) Propionate Additive and a Dopant-Free Polymer Hole Transport Material for CsPbI<sub>2</sub>Br Perovskite Solar Cells. *ACS Energy Letters* **2020**, *5*, 1292–1299.
16. Juarez-Perez, E. J., Ono, L. K., Uriarte, I., Cocinero, E. J. & Qi, Y. Degradation mechanism and relative stability of methylammonium halide based perovskites analyzed on the basis of acid–base theory. *ACS Applied Materials & Interfaces* **2019**, *11*, 12586–12593.
17. Liu, C.; Sun, X.; Yang, Y.; Syzgantseva, O. A.; Syzgantseva, M. A.; Ding, B.; Shibayama, N.; Kanda, H.; Fadaei Tirani, F.; Scopelliti, R. Retarding Solid-State Reactions Enable Efficient and Stable All-Inorganic Perovskite Solar Cells and Modules. *Science Advances* **2023**, *9*.
18. Iqbal, Z.; Félix, R.; Musiienko, A.; Thiesbrummel, J.; Köbler, H.; Gutierrez-Partida, E.; Gries, T. W.; Hüsam, E.; Saleh, A.; Wilks, R. G.; *et al.* Unveiling the Potential of Ambient Air Annealing for Highly Efficient Inorganic CSPBI3 Perovskite Solar Cells. *Journal of the American Chemical Society* **2024**, *146*, 4642–4651.
19. Ding, Y.; Guo, Q.; Geng, Y.; Dai, Z.; Wang, Z.; Chen, Z.; Guo, Q.; Zheng, Z.; Li, Y.; Zhou, E. A Low-Cost Hole Transport Layer Enables CsPbI<sub>2</sub>Br Single-Junction and Tandem Perovskite Solar Cells with Record Efficiencies of 17.8 % and 21.4 %. *Nano Today* **2022**, *46*, 101586.
20. Shan, S.; Xu, C.; Wu, H.; Niu, B.; Fu, W.; Zuo, L.; Chen, H. Manipulating the Crystallization and Phase Transition for High-performance CsPbI<sub>2</sub>Br Solar Cells. *Advanced Energy Materials* **2022**, *13*.
21. Xiang, W.; Liu, S. (Frank); Tress, W. A. Review on the Stability of Inorganic Metal Halide Perovskites: Challenges and Opportunities for Stable Solar Cells. *Energy & Environmental Science* **2021**, *14*, 2090–2113.
22. Xiang, W., Wang, Z., Kubicki, D. J., Wang, X., Tress, W., Luo, J., Zhang, J., Hofstetter, A., Zhang, L., Emsley, L., Grätzel, M., & Hagfeldt, A. BA-induced phase segregation and band



- gap reduction in mixed-halide inorganic perovskite solar cells. *Nature Communications* **2019**, *10*(1). DOI: 10.1039/D4EE02385D
23. Ozturk, T., Akman, E., Shalan, A. E., & Akin, S. Composition engineering of operationally stable CsPbI<sub>2</sub>Br perovskite solar cells with a record efficiency over 17%. *Nano Energy* **2021**, *87*, 106157.
24. Byranvand, M. M., Kodalle, T., Zuo, W., Magorian Friedlmeier, T., Abdelsamie, M., Hong, K., Zia, W., Perween, S., Clemens, O., Sutter-Fella, C. M., & Saliba, M. One-step thermal gradient- and antisolvent-free crystallization of all-inorganic perovskites for highly efficient and thermally stable solar cells. *Advanced Science* **2022**, *9*(23), 2202441.
25. Wang, P.; Wang, H.; Mao, Y.; Zhang, H.; Ye, F.; Liu, D.; Wang, T. Organic Ligands Armored ZnO Enhances Efficiency and Stability of CsPbI<sub>2</sub>Br Perovskite Solar Cells. *Advanced Science* **2020**, *7*.
26. He, J.; Liu, J.; Hou, Y.; Wang, Y.; Yang, S.; Yang, H. G. Surface Chelation of Cesium Halide Perovskite by Dithiocarbamate for Efficient and Stable Solar Cells. *Nature Communications* **2020**, *11*.
27. Shan, S.; Xu, C.; Wu, H.; Niu, B.; Fu, W.; Zuo, L.; Chen, H. Manipulating the Crystallization and Phase Transition for High-performance CsPbI<sub>2</sub>Br Solar Cells. *Advanced Energy Materials* **2022**, *13*.
28. Li, M. H., Shao, J. Y., Jiang, Y., Qiu, F. Z., Wang, S., Zhang, J., Han, G., Tang, J., Wang, F., Wei, Z., Yi, Y., Zhong, Y. W., & Hu, J. S. Electrical loss management by molecularly manipulating Dopant-Free Poly(3-hexylthiophene) towards 16.93 % CsPbI<sub>2</sub>Br solar cells. *Angewandte Chemie International Edition* **2021**, *60*(30), 16388–16393.
29. Liu, X.; Li, J.; Cui, X.; Wang, X.; Yang, D. The Progress and Efficiency of CsPbI<sub>2</sub>Br Perovskite Solar Cells. *Journal of Materials Chemistry C* **2023**, *11*, 426–455.
30. Han, Y., Zhao, H., Duan, C., Yang, S., Yang, Z., Liu, Z., & Liu, S. F. Controlled n-doping in air-stable CsPbI<sub>2</sub>Br perovskite solar cells with a record efficiency of 16.79%. *Advanced Functional Materials* **2020**, *30*(12), 1909972.
31. Zhang, W., Xiong, J., Li, J., & Daoud, W. A. Guanidinium passivation for air-stable rubidium-incorporated Cs<sub>(1-x)</sub>Rb<sub>x</sub>PbI<sub>2</sub>Br inorganic perovskite solar cells. *Solar RRL* **2020**, *4*(6), 2000112.
32. Zheng, K.; Ge, J.; Liu, C.; Lou, Q.; Chen, X.; Meng, Y.; Yin, X.; Bu, S.; Liu, C.; Ge, Z. Improved Phase Stability of CsPbI<sub>2</sub>Br Perovskite by Released Microstrain toward Highly Efficient and Stable Solar Cells. *InfoMat* **2021**, *3*, 1431–1444.



33. Yang, F.; Hirotani, D.; Kapil, G.; Kamarudin, M. A.; Ng, C. H.; Zhang, Y.; Shen, Q.; Hayase, S. All-inorganic CsPb<sub>1-x</sub>Ge<sub>x</sub>I<sub>2</sub>Br Perovskite with Enhanced Phase Stability and Photovoltaic Performance. *Angewandte Chemie International Edition* **2018**, *57*, 12745–12749. View Article Online  
DOI: 10.1039/D4EE02385D
34. Chaudhary, B.; Kulkarni, A.; Jena, A. K.; Ikegami, M.; Udagawa, Y.; Kunugita, H.; Ema, K.; Miyasaka, T. Poly(4-vinylpyridine)-based Interfacial Passivation to Enhance Voltage and Moisture Stability of Lead Halide Perovskite Solar Cells. *ChemSusChem* **2017**, *10*, 2473–2479.
35. Akel, S.; Kulkarni, A.; Rau, U.; Kirchartz, T. Relevance of Long Diffusion Lengths for Efficient Halide Perovskite Solar Cells. *PRX Energy* **2023**, *2*.

